Journal of Seismology **2**: 65–86, 1998.

On the cessation of seismicity at the base of the transition zone

Emile A. Okal & Craig R. Bina
Department of Geological Sciences, Northwestern University, Evanston, Illinois 60208, U.S.A.

Received 8 July 1997; accepted in revised form 5 February 1998

Abstract

Through a detailed analysis of seismicity at the base of the transition zone, we obtain an updated value of the maximum reliable depth of confirmed seismicity, we investigate regional variation in the maximum depth of seismicity among those Wadati-Benioff zones which reach the bottom of the transition zone, and we attempt to quantify the maximum possible rate of seismic release in the lower mantle compatible with the failure to detect even a single event since the advent of modern seismological networks. We classify deep subduction zones into three groups: those whose seismicity does not reach beyond 620 km, those whose seismicity appears to terminate around 650–660 km, and Tonga-Kermadec (and the 'Vityaz' cluster) whose seismicity extends to 685–690 km. We suggest that the depth extent of seismicity is controlled by the depth of the $\gamma \rightarrow pv + mw$ transition responsible for the '660-km' seismic discontinuity, which is deflected to greater depths in cold slabs than in warmer ones. We note that this transition marks the depth below which thermal perturbation of phase transitions no longer generates buoyancy anomalies and their large attendant down-dip compressive stresses and below which strain energy generated by other mechanisms may not accumulate to seismogenic levels due to superplastic weakness in fine-grained materials. We find that the maximum level of seismic activity in the lower mantle must be at least three orders of magnitude less than that observed in the transition zone.

Introduction and background

The purpose of this paper is to provide enhanced constraints on the cessation of seismicity around 690 km near the base of the transition zone. Our goal is severalfold: (i) to obtain an updated value of the maximum depth of reliably located global seismicity; (ii) to investigate the regional variation in the maximum depth of seismicity among those Benioff zones which do reach the bottom of the transition zone; and (iii) to attempt a quantification of the maximum possible rate of seismic release in the lower mantle which would be compatible with the failure to detect even a single event since the advent of the present seismological networks.

We are motivated in this endeavor by the fact that any theory for the origin of deep earthquakes must in particular explain their cessation at the bottom of the transition zone. In this respect, it is important to give as precise a figure as possible for the maximum depth of confirmed seismicity, and to study its variation among slabs. In addition, recent tomographic models generally indicate that at least some slabs do penetrate into the lower mantle (e.g., Van der Hilst et al., 1991, 1997), thus refuting the earlier argument that earthquakes are absent from the lower mantle simply because subduction itself stops at the bottom of the transition zone.

The unusual suggestion that earthquakes may actually occur in the lower mantle deserves some discussion. The idea of a global limit to the depth-extent of deep seismicity may, for example, be compared to apparent regional limits on the depth-extent of seismicity. In many areas of the world, seismicity stops at intermediate depths, even though we know from tomographic studies that the slab actually penetrates deeper than the maximum extent of seismicity. However, in several instances, a number of isolated, rare earthquakes have been documented beyond doubt at depths greater than the generally recognized limit of seismic activity in the relevant subduction zone. The most striking example is New Zealand where Adams (1963) and Adams and Ferris (1976) have identified the repeated occurrence of small events around 585 km depth, more than 270 km below the rest of the Wadati-Benioff Zone (hereafter WBZ), with a few more such

earthquakes taking place since the early 1990s. Similarly, in the South Sandwich Islands, two earthquakes occurred at the Northern (01 Jan 1979) and Southern (05 Oct 1997) ends of the arc, more than 100 km deeper than their closest neighbors. Thus, we must accept that exceptions to the general patterns of seismicity with depth in individual seismic zones are undeniable. Note that some of the very largest deep earthquakes (such as the Colombian earthquake of 1970, the Peruvian earthquakes of 1921–22 (Okal and Bina, 1994), or the Spanish earthquake of 1954 (Chung and Kanamori, 1976)) have occurred as isolated events taking place several hundred km below the apparent termination of the WBZ.

The occurrence of such situations raises the possibility that the observed aseismicity of the deep mantle may be an artifact of poor detection capabilities (both in terms of a magnitude threshold for detection at the surface and of a relatively short period of observation at an adequate detection level) and that an earthquake may one day be observed in the deep mantle. There is no compelling reason why the thermal regime of the slab should prohibit seismicity below depths of 690 km. The temperatures of the slab should not rise significantly at this depth; indeed, the endothermic nature of the transition from γ to $pv + mw$ should actually cool the slab in this depth range. With regard to mineralogical regime, certain proposed mechanisms for initiation of deep seismicity, such as transformational faulting or adiabatic instability, require the occurrence of kinetically delayed exothermic phase transitions, and these are much less likely to occur in lower mantle $pv + mw$ mineral assemblages than in shallower $\gamma + gt$ assemblages. However, there is no obvious mechanical or rheological reason why all potential mechanisms for seismic stress release should cease to operate in the lower mantle. On the other hand, if the lower mantle truly is aseismic, this may reflect a general absence of large deviatoric stresses below 690 km, rather than the absence of mechanisms for seismic stress release.

The depth of the deepest earthquakes: an update

In view of the abrupt cessation of seismicity at or around 700 km depth, a number of studies have addressed the question of the precise value of the maximum recorded depth of earthquakes. Among recent works, Stark and Frohlich (1985) have examined about 100 very deep events from the catalogue of the International Seismological Centre (ISC) covering the years 1964–1980 and concluded that none could be reliably located below 685 km on the basis of $pP - P$ readings. In addition, Rees and Okal (1987) have used International Seismological Summary (ISS) listings of historical earthquakes (1927–1963) whose original location was 670 km or deeper, and relocated 23 such events to depths less than or equal to 691 km. The precision of their relocations (estimated at 10 km) put their results in total agreement with Stark and Frohlich's (1985). However, they were unable to constrain the depth of 10 events, eight of which were not listed in the ISS. Our purpose here is to update these studies in several ways: (i) to investigate the post-1980 events which were listed by the National Earthquake Information Center (NEIC) at depths greater than 690 km; (ii) to complete the work of Rees and Okal (1987) by including data from the Bureau Central International de Séismologie (BCIS) compiled at Strasbourg, and not available to Rees and Okal; and (iii) to examine critically the depth of the deepest earthquakes in individual deep slabs to identify any regional variation in this parameter. We use the relocation method described in detail by Wysession et al. (1991), which is based on an interactive iterative least-squares algorithm; it also uses a Monte Carlo approach to systematically inject Gaussian noise (with standard deviation σ_G) into the data to study directly the level of resolution of the various variables (most critically depth in the present application). We use $\sigma_G = 1$ s for modern events, but larger values for historical ones.

Since the study of Stark and Frohlich (1985), eight events (all in the Fiji–Tonga subduction zone) have been assigned depths greater than 690 km by the NEIC. These are listed in Table 1 and discussed individually in the Appendix. Among them, five relocate between 562 and 685 km. Two more relocate at 709 and 710 km respectively, but with such poor depth resolution that hypocentral depths of 690 km are just as acceptable. The last event (19 May 1992) moves to 282 km when carefully relocated, as indicated by the ISC solution.

Among the historical events studied by Rees and Okal (1987), 10 earthquakes could not be relocated, for lack of adequate data. Having recently acquired a complete microfiche copy of the Bulletin of the BCIS, we were able to relocate eight of these earthquakes at depths ranging from 61 to 685 km. Among the remaining two, the event on 10 October 1957 relocates at 712 km, but with poor depth control, so that a solution at 690 km is just as acceptable. The dataset for the final event (14 July 1959) provides minimal depth resolution; this is a small aftershock of an event which

Table 1. Events postdating Stark and Frohlich's (1985) dataset with NEIC depths greater than 690 km

Date and Origin Time		NEIC hypocenter			ISC hypocenter			Relocated hypocenter (this study)					Magnitude
D M Y	GMT	Latit. °N	Longit. °E	Depth (km)	Latit. °N	Longit. °E	Depth (km)	Latit. °N	Longit. °E	Depth (km)†	Numb. of stations	σ (s)	m_b
12 04 1984	15:21	−24.124	179.004	694	−23.95	179.42	560	−23.95	179.49	562 F	10	0.82	4.6
10 01 1985	10:37	−18.039	−178.501	701	−18.1	−178.11	641	−18.10	−178.13	646 F	23	0.92	
22 10 1985	19:14	−20.158	−179.163	700	−20.23	−179.1	695	−20.19	−178.99	685 C	32	1.22	5.5
22 10 1985	19:29	−20.123	−179.309	707	−20.1	−179.3	707	−20.12	−179.18	690 C	17	0.76	
09 05 1989	13:24	−17.694	−179.091	692	−17.8	−179.1	693	−17.64	−179.04	685 F	11	0.74	4.5
08 11 1989	16:04	−19.695	−178.749	707	−19.7	−178.7	710	−20.29	−178.18	690 C	10	0.60	
19 05 1992	15:31	−21.974	−178.558	696	−19.5	−176.3	282	−19.43	−176.20	280 F	35	0.85	4.5
29 12 1992	12:46	−20.325	−178.949	695	−20.3	−178.3	665	−20.31	−178.26	664 F	8	0.82	4.4

†: F: Floating depth relocation; C: Monte Carlo relocations indicate no depth control; solution obtained with constrained depth.

relocates at 627 km, however, and the solution for the aftershock with the depth constrained at this value yields excellent residuals ($\sigma = 0.53$ s). Details on all these relocations are listed in the Appendix.

In conclusion, newly acquired data (in the form either of new events which occurred after the time window available to Stark and Frohlich (1985) or of BCIS bulletins complementing the dataset used by Rees and Okal (1987)) fully uphold the conclusions of these two studies: there are no earthquakes reliably located at depths greater than 690 km, with a precision estimated at 10 km.

Regional variation in the depth of the deepest earthquakes

In this section, we consider the regional variation of the maximum depth of earthquakes in those slabs whose seismicity does reach into the deepest part of the transition zone, namely below 620 km. Our goal in this work is to examine to what extent this maximum depth varies between slabs and which parameters may control any such variation. We refer to the previous works by Kostoglodov (1989) and Kirby et al. (1991, 1996), who introduced the notion of the thermal parameter, Φ, computed as the product of the age of the material in the slab and its vertical descent rate. These authors have observed that subduction zones for which $\Phi \leq 5\,000$ km do not exhibit deep earthquakes, while those with $\Phi > 5\,000$ km feature seismicity throughout the transition zone. We seek to refine the latter statement, specifically to determine if a further trend can be robustly identified on a small scale between thermal parameter and maximum depth among the deepest populations analyzed on Kostoglodov's (1989) Figure 2 or Kirby et al.'s Figures 9 (1991) or 4 (1996). Specifically, we investigate whether any trend exists in the maximum depth of seismicity between slabs with thermal parameters barely over 5 000 km (e.g., Java), those approaching 10 000 km (e.g., Marianas), and Tonga, whose Φ may be as large as 17 000 km. Following Marton et al. (1997), however, we caution that the definition of the thermal parameter may be inadequate in the case of the subduction of very old lithosphere, for which the thickness of the plate (which controls the rate of diffusion of heat into the cold slab) has tapered off to around 100 km (Parsons and Sclater, 1977; Stein and Stein, 1992) and is no longer a strong function of the age of the lithospheric material.

Since we are concerned only with the mechanism by which seismicity stops at the bottom of the transition zone, we do not consider here those slabs whose seismicity ceases above 600 km depth, and we thus restrict ourselves to the following subduction zones: Tonga-Kermadec, Solomon, Sangihe (Southern Philippines), Marianas, Java (West of 115°), East Sunda (East of 115°, including Banda Sea), Kuriles, Peru, Bolivia, and Argentina, as well as isolated events in Colombia and Northern Peru, Spain, and the detached 'Vityaz' slab under the North Fiji Basin. Note that with the exception of Solomon and Sangihe, where the tectonic regime is extremely complex and possibly transient, all the above slabs involve the subduction of 'old' plates, i.e., lithosphere having attained its maximum thickness beyond the age of 90 m.y. In terms of thermal properties, the main difference between these various zones

Table 2. Reassessment of historical events not relocated by Rees and Okal (1987)

Date and Origin Time	NEIC hypocenter			BCIS(*) hypocenter			Relocated hypocenter (this study)					Remarks;
D M Y GMT	Latit. N	Longit. °E	Depth (km)	Latit. °N	Longit. °E	Depth (km)	Latit. °N	Longit. °E	Depth (km)	Numb. of stations	σ (s)	Action taken
12 08 1933 09:25	−6.0	121.0	720	−1.7	122.7	33 I	−6.1	120.8	607 F	9	2.56	Increase Amboina by 1 mn; no depth control
20 12 1939 13:04	−7.0	120.0	700	No location			−6.95	121.10	623 F	11	1.95	Poor depth control
13 11 1954 14:46	30	131.8	800	30	131.8	80	29.83	131.60	62 F	17	1.92	Typographic error
18 11 1954 12:46	42.25	141.6	800	42.25	141.6	80	42.09	141.65	89 F	14	1.52	Typographic error
21 01 1956 13:37	−1.5	129.5	700	−1.5	129.5	700	−5.49	130.08	186 F	8	0.75	Increased P at BRS by 1 mn; Decreased S at MAT by 1 mn.
12 03 1957 17:21	−21.5	−179.0	700	−21.5	−178	700	−21.12	−178.79	681 F	19	2.67	Use BCIS data
10 10 1957 03:47	−22.0	178.5	700	−22	178.5	700	−22.17	178.52	690 C	18	1.57	Use BCIS data
14 07 1959 18:20	−21	−179.0	700	−21	−179	700	−20.91	−179.13	627 C	5	0.53	Constrain depth to same as main shock
07 04 1960 03:05	−21.37	−179.29	670	−21	−179.5	600	−21.29	−179.07	585 F	9	1.53	Use BCIS data; eliminate RIV, SHL
11 11 1960 06:14	−19.84	−179.05	670	'discordant data'			−19.80	−179.01	666 F	12	0.72	Increase CAN and CTA by 1 mn; eliminate BHA

†: F: Floating depth relocation; C: Monte Carlo relocations indicate no depth control. Solution obtained with constrained depth.
(*): I: ISS solution when no BCIS one is available.

will arise from their rate of subduction, not from the absolute age of the material being subducted.

In the subsequent paragraphs, we investigate the maximum depth of seismicity in each of these subduction zones, based on the following datasets: the computerized NEIC dataset; ISC inverted hypocenters, generally available after 1963 (most often with a precision estimate); ISC hypocenters estimated from $pP-P$ (generally available for larger events); centroid depths from the inversion of moment tensors (Dziewonski et al., 1983, and subsequent quarterly updates for events postdating 1976, available for $M_0 \geq 10^{24}$ dyn-cm; Huang et al., 1997 for WWSSN solutions, available for $M_0 \geq 2 \times 10^{25}$ dyn-cm); depths inverted by Engdahl et al. (1997), available for larger events and during 1964–1991. In the case of smaller events for which few depth estimates were available, we conducted our own relocations (including Monte Carlo tests) based on ISC or BCIS listings. We also include results from a few historical events, when the latter are significant or their discussion relevant. All data are listed in Table 3. Preliminary results of the present study were included in

Table 3. Deepest events in Deep Wadati-Benioff Zones (1962–1995)

Date		Magnitude	Depth (km)							Remarks
D M Y	[hh:mm]	m_b	NEIC (Inverted)	ISS/ISC pP	ISS/ISC (†)	CMT Study	This Carlo	Monte (†)	EHB	
			Java [10° S–3° S; 105° E–115° E]							
09 08 1983		5.2	655	658 ± 3		656 D			646	
04 10 1994		5.0	652	648 ± 13						
15 12 1963		6.4	650	654		661 H				
08 06 1977		5.1	643	637 ± 4	634				639	
18 10 1986		5.7	643	655 ± 6	648	645 D			646	
28 09 1994		5.9	637	660 ± 6	635	653 D				
			Conclusion: Seismicity stops around 660 km							
			East Sunda including Banda Sea [10° S–3° S; 115° E–130° E]							
06 02 1963			665				609	512–673		
14 06 1966		5.4	660	617					635	
26 10 1992		4.7	657	650 ± 10						
01 08 1984		5.1	657	657 ± 3		656 D			639	
16 02 1967		4.7	652	663 ± 11			663	637–700	641	
21 11 1987		5.1	651	651		609 D			634	
30 05 1995		5.3	630	650 ± 5		670 D				Deepest CMT solution (6.6×10^{23})
11 05 1955			700				684	627–753		Rees and Okal (1987): 691 km
			Conclusion: Seismicity stops around 660 km							
			Solomon Islands [8° S–3° S; 150° E–160° E]							
22 04 1991		4.8	626	624 ± 24			627	580–656		Only event below 620 km
15 12 1976		4.9	608	608 ± 3					603	
23 06 1982		4.4	599	597 ± 3					590	
12 07 1995		4.8	595							
03 10 1993		4.5	590	584 ± 7						
10 08 1994		4.8	590	590 ± 7						
			Conclusion: Seismicity stops around 605 km							
			Sangihe–South Philippines [2° N–10° N; 120°–128° E]							
25 04 1969		4.8	660	664 ± 4			662	646–676	651	Deepest NEIC-reported
19 08 1988		4.6	658	660 ± 23			633	601–658		
25 01 1993		4.6	656	657 ± 13			661	640–678		
05 03 1984		6.5	649	656 ± 2	665	644 D			658	Deepest large event
			Conclusion: Seismicity stops around 660 km							
			Mariana Islands [10° N–20° N; 140° E–150° E]							
07 03 1962		7.0	685	689		661 H	672	654–688		Stark and Frohlich: 655–680 km
12 11 1993		4.6	656	659 ± 5						
12 10 1963		4.0	638				578	539–608		
19 11 1978		4.3	621	629 ± 9			617	585–643		
23 02 1968		4.8	620	625 ± 4					626	
			Conclusion: Seismicity stops around 660 km							

Table 3. (continued)

Date		Magnitude	Depth (km)							Remarks
D M Y	[hh:mm]	m_b	NEIC (Inverted)	ISS/ISC pP	ISS/ISC (†)	CMT Study	This Carlo	Monte (†)	EHB	
		Kuriles–Kamchatka [42° N–55° N; 140° E–160° E]								
14 08 1988		5.4	645	632 ± 5	645	649 D			651	
30 08 1970		6.6	645	643 ± 3	648	650 H			640	
02 04 1986		4.4	630	618 ± 16			612	593–644	602	
22 08 1966		5.1	630	626 ± 2	637				639	
27 11 1982		5.6	622	619 ± 2	638	628 D			641	
		Conclusion: Seismicity stops around 650 km								
		Argentina [30° S–13° S; 66° W–55° W]								
01 01 1968		3.9	641	599 ± 12			609	576–632		
26 04 1984		5.3	623	623 ± 3					614	
03 12 1972		4.5	621	628 ± 8			623	595–645		
08 12 1962		6.5	620	582		589 H			600	
		Conclusion: Seismicity stops around 620 km								
		Bolivia [15° S–12° S; 71° W–66° W]								
09 06 1994	01:15	6.1	650							
23 06 1994		4.4	642	655 ± 8	640					
10 01 1969		4.0	636	661 ± 5			664	645–686		
09 06 1994	00:33	7.0	631	640 ± 4	713	647 D				
09 06 1994	05:26	5.2	630	664 ± 5						
10 06 1994		4.3	629	636 ± 8						
		88 aftershocks located by Myers et al. (1995) from 622 to 660 km, plus one at 665 km								
		Conclusion: Seismicity stops around 660 km								
		Peru–Brazil [12° S–7° S; 73° W–70° W]								
23 04 1987		3.7	674	672 ± 27			665	613–696		
28 11 1964		5.6	655	650 ± 5	638	627 H			642	
11 07 1978		5.8	645	643 ± 3	636	628 D			634	
28 11 1964		5.4	626	651 ± 4	637				641	
09 07 1950		7.0	650	667		649 H				Significant historical event
		Conclusion: Seismicity stops around 650 km								
		Tonga [35° S–15° S; 175° E–175° W]								
07 05 1971				848 ± 0.2			624	577–657		All-time deepest ISC solution
25 10 1972				806 ± 0.8			433	400–463		Second-deepest ISC solution
31 10 1977			734	734			738	44–800		Deepest NEIC-reported; no depth control
08 11 1989			707		See Table 1					
22 10 1985	19:29		707		See Table 1					
10 01 1985			701		See Table 1					
22 10 1985	19:14	5.5	700		See Table 1					
12 01 1969		4.2	697	697 ± 17			689	544–773		
19 05 1992		4.5	696		See Table 1					
07 12 1978			695	625 ± 6			626	607–641		

Table 3. (continued)

Date		Magnitude	Depth (km)							Remarks
D M Y	[hh:mm]	m_b	NEIC	ISS/ISC (Inverted)	ISS/ISC pP	CMT (†)	This Study	Monte Carlo	EHB (†)	
		Tonga (continued)								
11 12 1978		4.8	695	608 ± 9			608	581–631		
25 09 1971		4.6	695	694 ± 7			694	671–715	687	Deepest event in Engdahl et al.
29 12 1992		4.4	695	See Table 1						
12 04 1984		4.6	694	See Table 1						
09 05 1989		4.5	692	See Table 1						
17 01 1975		4.6	692	602 ± 7			603	585–627	586	
17 06 1977		5.7	690	673 ± 6	684				679	
10 10 1984		5.6	676	676 ± 3	679	691 D			670	
22 10 1985	19:13	5.0	686	690 ± 9	690	684 D			676	
		Conclusion: Seismicity reaches 690 km								
		Northern Peru–Colombia [5° S–1° S; 75° W–70° W]								
18 12 1921		7.9 GR	650	540			630			(Okal and Bina, 1994)
17 01 1922		7.6 GR	650	0		664 H	660			(Okal and Bina, 1994)
31 07 1970		7.1	651	653 ± 3	645	623 R				
		Conclusion: Seismicity stops around 660 km								
		Spain [35° N–40° N; 5° W–0° W]								
29 03 1954		7.0	640	603			627	616–637		Rupture propagated 20 km downwards (Chung and Kanamori, 1976)
30 01 1973		4.0	634	636 ± 3			633	623–644		
31 07 1993		3.9	626	631 ± 21						
08 03 1990		4.1	625	624 ± 4						
			Conclusion: Seismicity stops around 650 km							
		Vityaz Cluster [16° S–11° S; 167° E–177° E]								
28 08 1961		$6\frac{1}{2}$	640				664	641–696		
24 04 1966		4.4	660	663 ± 6					656	
20 05 1976		4.3	661	661 ± 4			662	642–681		
17 03 1977	09:17	4.9	657	663 ± 7			661	643–676	642	
17 03 1977	09:18	4.8	652	664 ± 8			660	644–674	648	
17 03 1977	12:42	5.0	649	662 ± 5					645	
12 08 1979		4.2	650	673 ± 10			674	642–705	653	
14 12 1979		4.6	683	664 ± 5					649	
23 01 1981		4.4	654	660 ± 5					641	
03 11 1981		4.8	654	660 ± 5					647	
09 07 1984		4.7	669	670 ± 5			670	649–685	651	
08 09 1984		4.1	681				681	570–727		
13 11 1984		4.0	676	672 ± 10			670	604–719		
01 12 1984	14:13	4.8	677	679			677	659–702	654	
01 12 1981	14:18	5.1	673	675			672	653–689	651	
23 01 1985		4.6	663	662 ± 14			661	583–717		
24 01 1986		5.2	663	660 ± 7					641	

Table 3. (continued)

Date		Magnitude	Depth (km)							Remarks
D M Y	[hh:mm]	m_b	NEIC	ISS/ISC (Inverted)	ISS/ISC pP	CMT (†)	This Study	Monte Carlo	EHB (†)	
		Vityaz Cluster (continued)								
07 09 1986		4.9	665	664 ± 7		671 D			652	
08 09 1986		4.8	641	664 ± 7					650	
06 08 1987	09:52	4.9	659	660 ± 9					644	
06 08 1987	11:39	4.8	654	683			664	466–753		
11 12 1988		4.2	613	666 ± 45			666	564–740		
24 01 1990		4.6	680	609 ± 49			683	633–776	666	
		Conclusion: Seismicity stops around 672 km								
		Other event								
16 12 1977		(Japan Sea)	637	380			540	325–800		No depth resolution NEIC probably erroneous

† D: Harvard CMT (Dziewonski et al., 1983 and subsequent quarterly updates); H: Huang et al. [1997]; R: Russakoff et al. (1997). EHB: Engdahl et al. (1997).

the review of deep seismicity by Kirby et al. (1996). The precision sought in these descriptions is never better than ±10 km.

Table 3 shows that there exists a systematic, but not universal, trend for Engdahl et al.'s (1997) relocations to be shallower than the ISC and NEIC solutions and than our own relocations. As discussed in greater detail by Van der Hilst and Engdahl (1992) and Engdahl et al. (1997), this reflects a combination of the use of Kennett et al.'s (1995) model 'ak135' as opposed to Jeffreys and Bullen's (1940) Tables, the non-random distribution of stations, and the use of use of depth phases (mostly pP) by Engdahl et al. (1997), which compensates to some extent the bias introduced by propagation of a significant fraction of rays through fast material in subducting slabs. At any rate, the magnitude of this trend is less than the precision sought in the present study.

We also take this opportunity to emphasize that there remains a small level of potential incompleteness in the various tables we present. Our procedure does not guard against the possibility that an event listed as shallow by all cataloguing agencies (NEIC, ISC, etc.) could actually be among the deepest in a subduction zone. The only perfectly foolproof approach to this problem would be to re-examine every single earthquake of any depth recorded since the beginning of reliable bulletins (ca. 1920). This herculean task is clearly beyond the scope of the present study, but some perspective can be found in Engdahl et al.'s (1997) relocation catalogue: out of a total of 99 510 entries, these authors list only 11 earthquakes with shallow catalogue foci (constrained at 0 or 33 km in all cases) which they relocated in the transition zone ($h \geq 400$ km), none of them at the tip of the WBZ.

Java

The combination of precise ISC locations and CMT inversions suggests that seismicity stops around 660 km, although Engdahl et al.'s (1997) relocations would place the deepest earthquakes about 10 km shallower.

East Sunda Arc including Banda Sea

The combination of precise ISC locations, CMT inversions and our own relocations places the deepest earthquakes around 660 km, although again, Engdahl et al.'s hypocenters are 15 km shallower. The only exceptions are the 1963 NEIC listing, for which our study suggests very poor depth resolution. The figure of 660 km is also in general agreement with the results of Rees and Okal (1987), who studied seven historical earthquakes in this area. Only their solution for 11 May 1955 was significantly deeper (691 km), but Monte Carlo tests show very poor depth resolution for this event.

Solomon Islands

Because there is only one Solomon Islands hypocenter listed below 620 km by the NEIC (22 April 1991, 626 km; $m_b = 4.8$), we include in Table 3 all earthquakes below 590 km in this region. The 1991 earthquake is listed by the ISC at an equivalent depth (627 km); however, our Monte Carlo relocations on the available dataset of only 10 stations range from 589 to 656 km, indicating mediocre depth control. Seismicity is otherwise documented robustly in the 600 to 610 km range, and there is no reason to believe that the 1991 earthquake is any deeper. The maximum depth of seismicity in the Solomon Islands is taken as 605 km.

Sangihe–South Philippines

All available information indicates that seismicity ceases around 660 km, including well constrained ISC locations (25 Apr 1969; 05 Mar 1984), Engdahl et al.'s (1997) relocations (05 Mar 1984), and our own Monte Carlo tests (25 Apr 1969; 25 Jan 1993). This figure is also in agreement with the work of Rees and Okal (1987), who found a maximum depth of 662 km for the Mindanao earthquake of 22 Sep 1940.

Mariana Islands

The case of the Mariana WBZ is somewhat singular in that the deepest reported event (07 Mar 1962, 685 km (NEIC)) is also one of the largest in that slab below 500 km. While the NEIC and ISC report it as very deep, both our relocations and Stark and Frohlich's (1985) suggest a somewhat shallower depth around 670 km. Furthermore, a relocation constrained at the inverted centroid (661 km, Huang et al. (1997)) is not significantly deteriorated with respect to our best hypocenter ($\sigma = 1.43$ s as opposed to 1.40). We therefore adopt the figure of 665 km for the maximum depth of seismicity in the Marianas, while remembering that it reflects the average of various estimates for a single earthquake.

Kuriles–Kamchatka

The various datasets are very consistent, notably regarding the great 1970 deep shock, and suggest a maximum depth of 650 km for this WBZ.

Argentina

Since 1962, only 4 earthquakes were reported at or below 620 km by the NEIC. Of those, the small 1968 earthquake (641 km) has very poor depth resolution, but is most probably much shallower, and the large 1962 earthquake is most certainly no deeper than 590–600 km. The reasonably robust event in 1984 suggests 620 km as the maximum depth of seismicity under Argentina.

Bolivia

The case of this segment of the South American subduction zone is special, since its seismicity consists nearly exclusively of the great 1994 event and its aftershocks. The extensive study by Myers et al. (1995) indicates a maximum depth of 660 km (except for a lone event at 665 km, for which no estimate of precision is given).

Peru–Brazil

Precise NEIC and ISC relocations suggest 650 km as a maximum depth, although the other sources would argue for a figure 10 km shallower. The dataset for the small 1987 event has poor resolution, and its greater depth is not robust. The centroid for the large 1950 shock (649 $\pm$ 8 km) also supports a maximum depth of 650 km, as do the results of Rees and Okal (1987) on the shocks of 26 Nov 1945 (640 km), 18 Sep 1950 (647 km) and 28 Dec 1950 (657 km).

Tonga–Kermadec

As detailed in numerous studies (Giardini, 1984; Stark and Frohlich, 1985; Rees and Okal, 1987; Engdahl et al., 1997), there is ample evidence that seismicity reaches 685 km, and a few earthquakes are well documented at 690 km in the Tonga–Kermadec subduction zone, these figures having an uncertainty of about $\pm$5 km (e.g., 25 Sep 1971, 22 Oct 1985 (19:13)). We refer to Table 1 and the discussion in the previous section regarding post-1980 events reported deeper than this figure.

We also examined in detail a few earthquakes described by Stark and Frohlich (1985) with reported depths greater than 690 km. The most puzzling cases are the two ISC reports for 07 May 1971 at 22:30 (848 km) and 25 Oct 1972 (806 km). Neither shock is reported by the NEIC; however, our relocations move

these events to hypocenters at 624 and 433 km, respectively, with Monte Carlo depths reasonably constrained to the intervals 574–664 km and 400–463 km. Also, the 1971 earthquake appears to be an aftershock of a previous shock, occurring three hours earlier, given by the NEIC at 606 km, by the ISC at 664 km, and which we relocate at 575 km. We are at a loss to figure out the origin of those exceedingly deep ISC solutions, in view of the existence of much shallower satisfactory solutions. The nearly coeval character of these two instances, and the fact that they did not recur in the next 22 years, as well as the unrealistic error bars in the ISC solutions, would suggest a change of algorithm in the ISC computation, with the application of more stringent quality control some time after 1972.

The situation with the deepest NEIC solution (31 Oct 1977) is somewhat different in that all inversions locate it around 730 km, but the solution has absolutely no depth resolution, as indicated by our Monte Carlo tests (the maximum Monte Carlo depth is artificially constrained at 800 km in our program). Thus, we confirm that the exceedingly deep foci reported by the NEIC and ISC are artifacts of datasets with poor resolution, unstable location algorithms or both.

Isolated shocks: Northern Peru and Colombia; Spain

In these two regions, a few, rare, isolated earthquakes are documented at the bottom of slabs which are otherwise inactive below 300 and 150 km, respectively. Because of the rarity of these events, we cannot regard their hypocenters as marking precisely the depth of maximum seismicity in the relevant regions. However, it is interesting to note that in both instances these shocks seem to take place in (or their source regions to extend to) the immediate vicinity of the maximum depth of activity commonly identified in many other subduction zones (650 to 660 km). Specifically, in Northern Peru and Colombia, only three large shocks are known; the depth of the 1970 earthquake is constrained to within a few km of 650 km; as for the 1921 and 1922 events, Okal and Bina (1994) have proposed depths of 630 and 660 km, respectively. In Spain, only three small events have been detected in the vicinity of the 1954 large deep earthquake. The latter's hypocenter is very well constrained to 630±3 km, with a downward rupture extending to 649 km (Chung and Kanamori, 1976). As for the smaller events, their depths are comparable.

The Vityaz cluster

This group of earthquakes, located deep under the North Fiji Basin, has recently been investigated by Kirby and Okal (1996), who interpret them as occurring in the remnant of a so-called Vityaz slab, lying recumbent at the bottom of the transition zone. The slab subducted southwestwards under the Australian plate until 8 million years ago, when it was deactivated as part of the reorganization of the plate boundary system in the region (Chase, 1971; Hamburger and Isacks, 1987). As detailed in Table 3, well constrained ISC and NEIC solutions are found regularly at a maximum depth of about 665 km, with one well constrained event at 672 km (01 Dec 1981, 14:18) and two more at 674 (12 Aug 1979) and 677 km (01 Dec 1984, 14:13); note however that Engdahl et al. (1997) would place these events about 20 km shallower. As for those events located deeper (down to 683 km) by Okal and Kirby (1996), they have much poorer depth resolution, as indicated by our Monte Carlo tests. We use 672 km as the maximum depth of seismicity in the Vityaz cluster.

Other event

Finally, the NEIC tape lists one event below 620 km belonging to neither of the above slabs, namely under the Sea of Japan on 16 Dec 1977 (33.0° N, 136.4° E, 637 km). The ISC lists it at 380 km, and our relocation converges on 543 km; however, the dataset has little depth resolution, and the earthquake can be accommodated between 330 and 410 km, the range of robust solutions in that part of the Honshu slab.

Discussion

The pattern emerging from the above study is that of relatively discontinuous behavior of the depth of maximum seismicity among those WBZs reaching the deepest parts of the transition zone. These can be classified into three groups. Group (i) consists of those subduction zones whose seismicity does not reach beyond 620 km: Solomon, Argentina. Group (ii) contains a large set of deep subduction zones for which there is documented seismicity below 620 km and whose WBZs all seem to terminate around 650–660 km: Sangihe, Banda Sea, Java, Kuriles, Bolivia, Peru-Brazil. The maximum depth in the Marianas, 665 km, is not significantly greater than this figure, and the isolated seismicity in Colombia-Northern Peru and Spain also fits this general pattern. Note that this set

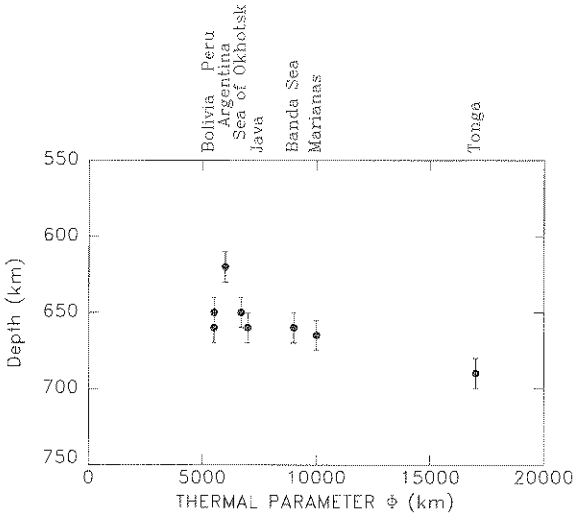

Figure 1. Deepest seismicity in deep-reaching subduction zones, as compiled from the data in Table 3, as a function of their subduction thermal parameter, Φ. The latter are taken mainly from Kirby et al. (1991), with parameters for the Tonga and the South American segments adjusted in the light of new data (Bevis et al., 1995) or models (Engebretson and Kirby, 1992). Sangihe and Solomon trenches not included for lack of precise kinematic model, nor are the detached Vityaz slabs and the isolated events of Spain and Colombia.

regroups subduction zones with thermal parameters varying between 5 000 and 10 000 km as documented in Kirby et al. (1996). In other words, and as illustrated on Figure 1, there is no apparent influence of Φ on the maximum depth of seismicity for this group. Group (iii) consists of the Tonga–Kermadec subduction zone, whose seismicity extends down to 685–690 km, as well as the seismicity of the deep, probably recumbent 'Vityaz' cluster below the Northern Fiji Basin (maximum depth 672 km).

These observations strongly suggest that, within a well developed, mature subduction zone, the depth extent of seismicity is controlled by the depth of the second mantle discontinuity. The latter should be about 660 km in undisturbed mantle; due to its negative Clapeyron slope (Navrotsky, 1980), the equilibrium $\gamma \rightarrow pv + mw$ transition is deflected to greater depths within the thermal fields of colder slabs than in those of warmer slabs. If, following Kirby et al. (1996), we adopt $\sim$ 300 K as a representative temperature difference, at $\sim$ 660 km depth, between a slow, relatively young slab (such as Java), which will be 'warm' (if not 'hot') among the slabs whose seismicity reaches the bottom of the transition zone, and a very fast, very old and therefore very cold one (such as Tonga), and if we assume an effective Clapeyron slope of -3 ± 1 MPa/K for the $\gamma \rightarrow pv + mw$ transition (Bina and Helffrich, 1994), we find that the transition in the cold slab will be deflected by an additional 900 ± 300 MPa in pressure, or $\sim 27 \pm 9$ km in depth, relative to the transition in the warm slab (Figure 2). This is in remarkable agreement with our observation that deep seismicity in the Tonga subduction zone extends 25–30 km below that in other, warmer subduction zones.

The case of the only other zone of seismicity consistently deeper than 660 km, the Vityaz cluster, is more complex. The most probable model for its origin leaves little doubt that the material is composed of very old lithosphere, having come from the long-defunct Phoenix Ridge (Engebretson et al., 1991), but we can only speculate on its velocity of subduction. The mechanical separation of the recumbent piece of slab from the Pacific plate's lithosphere may have resulted in much faster sinking (at least initially), which could conceivably leave the seismogenic material significantly colder than the adjoining mantle. Meanwhile, in all other subduction zones, the downward deflection of the discontinuity would remain less than 15 km and thus probably within the uncertainty of our estimates of maximum depth.

In the previous section, we have presented phenomenological evidence suggesting that the depth of maximum seismicity appears to be controlled by the depth of the second mantle transition in individual subduction zones. In attempting to explain why this might be so, three possible explanations are immediately evident: (1) an appropriate mechanism of seismic release (e.g., transformational faulting, dehydration, partial melting) cannot operate at greater depths, (2) material strengths below these depths are too low to permit the accumulation of strain energy to potentially seismogenic levels, or (3) there are no large stresses generated beyond these depths which would engender seismic release. With regard to seismic release (1), while certain proposed mechanisms (e.g., transformational faulting, adiabatic instability) require the occurrence of kinetically retarded exothermic phase transitions which are unlikely to occur in the lower mantle, we know of no compelling reason that all potential mechanisms of seismic stress release should suddenly cease to be viable below the depth of the $\gamma \rightarrow pv + mw$ transition. However, given the uncertainty surrounding the operative mechanisms of seismic release even at shallower depths, we cannot rule out this possibility.

With regard to strain accumulation (2), while olivine grows progressively less able to store strain energy for seismogenesis with increasing temperatures

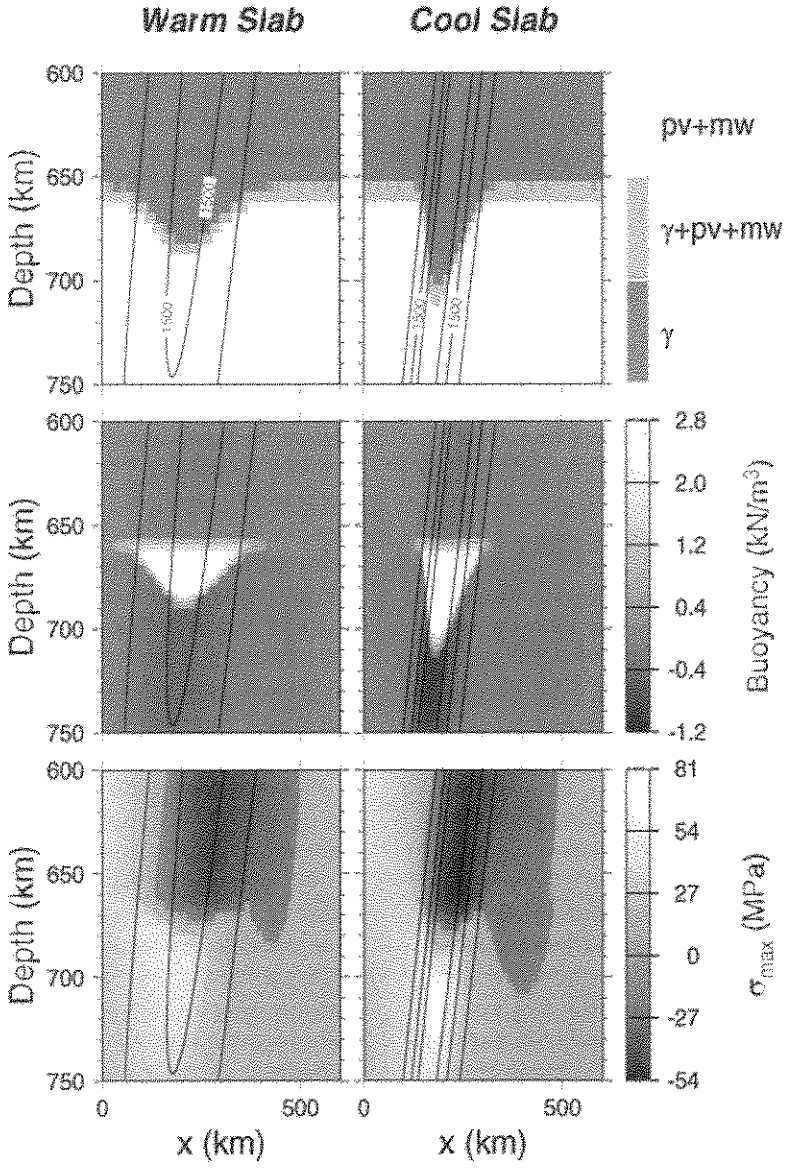

Figure 2. Equilibrium depth of the $\gamma \rightarrow pv + mw$ transition (top), corresponding buoyancy anomalies (middle), and consequent (absolute) maximum principal stresses (bottom; negative = compression) for warm (left) and cold (right) slabs. The 1500 K isotherm is labeled and adjoining ones at 300 K intervals shown. Vertical exaggeration is 4:1.

due to its declining strength, transition zone minerals such as the β and γ phases are significantly stronger than olivine (Weidner, 1997). However, the $pv + mw$ assemblage produced below the '660-km' discontinuity should be fine-grained, possibly producing a weak superplastic zone which is incapable of storing seismogenic elastic energy (Ito and Sato, 1991), a hypothesis which is consistent with the absence of observed seismic anisotropy in the lower mantle (Karato, 1998). Moreover, while any potentially seismogenic adiabatic instabilities occurring at moderate slab temperatures would be promoted by the high strain rates induced by such grain-size reduction, such instabilities would be terminated by negative latent-heat release at the 660-km transition (Karato, 1997). Thus, it is plausible that strain energy may accumulate less efficiently below the $\gamma \rightarrow pv + mw$ transition.

With regard to stress generation (3), a case can be made as to why there should be no large stresses to be released seismically at depths below the $\gamma \rightarrow pv + mw$ transition. The cold thermal field of the slab acts to deflect the equilibrium depths of the $\alpha \rightarrow \beta \rightarrow \gamma$ transitions upwards while (Figure 2) deflecting the deeper $\gamma \rightarrow pv + mw$ transition downwards (Schubert et al., 1975). The attendant buoyancy anomalies result in large down-dip compressive stresses in the region between these phase transitions, which are reflected in the distribution and mechanisms of deep earthquakes (Ito and Sato, 1992; Bina, 1996). Below the $\gamma \rightarrow pv + mw$ transition, however, there is no such mechanism for generating large compressive stresses through opposed buoyancy anomalies, and the slab reverts to small tensional stresses (Bina, 1997). These tensional stresses fall off rapidly with depth because the negative thermal buoyancy of the slab decreases as the slab thermally equilibrates with increasing depth of penetration, and they are of significant magnitude only immediately below the $\gamma \rightarrow pv + mw$ transition. No down-dip tensional seismicity is known from this region, and any slab bending (Lundgren and Giardini, 1992; Van der Hilst, 1995) in response to the buoyancy forces or any encounter with putative viscosity increases (King, 1995) would counteract these tensional stresses. (The region of large compressive stress outside the thermal halo of the slab in Figure 2 arises from gravitational loading of the inclined slab on the underlying mantle material and occurs where the mantle is too warm to support seismicity.) Thus, as the equilibrium depth of the $\gamma \rightarrow pv + mw$ transition increases (linearly) in colder slabs, the depth to the corresponding cutoff in down-dip compressive stress also increases (nonlinearly).

In summary, the $\gamma \rightarrow pv + mw$ transition occurs at a greater equilibrium depth in colder than in warmer slabs, and this transition marks the depth below which buoyancy anomalies no longer generate the large down-dip compressive stresses associated with seismicity. Furthermore, any stresses generated by other mechanisms may be unable to accumulate seismogenic levels of strain energy below this transition, due to the probable formation of a fine-grained, weak, superplastic zone in the $pv + mw$ stability field. Thus, the depth of cessation of seismicity should be greater for colder slabs than for warmer ones, just as we observe.

Quantifying the maximum possible moment release in the deep mantle

Just how aseismic is the deep mantle? We have yet to confidently locate a single earthquake below 690 km depth, but one cannot exclude the possibility that some seismicity could be present at greater depths, either at low magnitudes escaping detection at the surface or taking place too infrequently to have been observed since the inception of the world-wide seismograph network in the early 1960s. In this section, and based on a few hypotheses on detection thresholds and frequency-size relations, we derive an estimate of the maximum possible level of moment release rate of such undetected events in the deep mantle, below the transition zone. For the purpose of comparison with seismicity in the transition zone, we will use as a reference period the time window 1977–1995 which, as of the date of writing, constitutes the latest full-year span of the Harvard centroid moment tensor solutions (Dziewonski et al., 1983, and subsequent quarterly updates).

The threshold of completeness for the observed aseismicity of the deep mantle

We must first assess the moment threshold above which we can confidently claim that no earthquake has occurred in the deep mantle during the reference period. Detection capabilities are directly related to the amplitude of body waves excited by a source with a given seismic moment. In turn, this is controlled by several terms (e.g., Okal, 1992), primarily the far-field P-wave excitation coefficient $1/\rho\alpha^3$ and the geometrical spreading factor $g(\Delta, h)$. We have verified that at a given distance Δ, these terms will be only very slightly affected when sinking the source below the 670-km discontinuity: the change of amplitude for a P-wave would correspond to less than 0.1 unit of magnitude (Okal, 1993). As a result, detection capabilities are expected to be similar at the bottom of the transition zone and in the lower mantle, taken here as the depth range $690 < h \leq 1000$ km. In the case of the very deepest transition zone earthquakes (600–690 km), Okal and Kirby (1995, Figure 5) have shown that the frequency-size relationship is linear down to 10^{24} dyn-cm, suggesting that the dataset is complete down to that value, and we can therefore state confidently that no earthquake of moment $M_0 \geq 10^{24}$ dyn-cm located in the lower mantle would have escaped detection during the CMT era. We will use this value

(10^{24} dyn-cm) for M_{thresh}, the threshold of completeness for the aseismicity of the deep mantle.

Modeling the frequency-size distribution of possible seismic events in the lower mantle

It is obviously very difficult to propose a model for a population of which no member has ever been observed. In this endeavor, we assume that potentially seismogenic material in the deep mantle would take the form of blobs, whose fractal dimension can be taken as 3 (as in the transition zone), as opposed to 2 in the case of shallow earthquakes distributed on faults. We further assume that deep-mantle earthquakes would involve shear faulting on a planar surface, so that the familiar relation $M_0 = \mu S\,\Delta u$ would hold, and that the physical saturation of earthquake source dimensions would involve the same regimes as for transition zone shocks. In other words, we make here the uniformitarian assumption that the properties of seismic events in the lower mantle would be comparable to those in the transition zone, as studied by Okal and Kirby (1995). Under these conditions, we consider a population of deep mantle earthquakes with a frequency-moment distribution following a three-tier law of the form

$$\begin{aligned}
&\log_{10} N = a_1 - \beta_1 \log_{10} M_0 \quad \text{for} \quad M_0 \geq M_1 \\
&\log_{10} N = a_2 - \beta_2 \log_{10} M_0 \quad \text{for} \quad M_2 \leq M_0 \leq M_1 \quad (1) \\
&\log_{10} N = a_3 - \beta_3 \log_{10} M_0 \quad \text{for} \quad M_0 \leq M_2.
\end{aligned}$$

By comparison with transition zone earthquakes, and based on fractal dimensionality arguments, we take $\beta_1 = \beta_3 = 1$; $\beta_2 = 1/2$. Then, in order to ensure continuity at the corner moments M_1 and M_2,

$$a_1 = a_3 + \frac{1}{2}\log_{10}\frac{M_1}{M_2}, \qquad a_2 = a_3 - \frac{1}{2}\log_{10} M_2 \quad (2)$$

where the constants a_i would depend on the particular reference time window.

The total seismic moment release in a moment window $\{M_{\min}; M_{\max}\}$ spanning the three regimes is simply given by

$$\begin{aligned}
[M_0]^{\max}_{\min} &= \int_{M_0=M_{\min}}^{M_0=M_{\max}} M_0(-dN) \\
&= 10^{a_3}\cdot \ln\frac{M_2}{M_{\min}} + 10^{a_2}\cdot\left(\sqrt{M_1}-\sqrt{M_2}\right) \\
&\quad + 10^{a_1}\cdot \ln\frac{M_{\max}}{M_1} \qquad (3)
\end{aligned}$$

Over the length of the reference period, $\tau = 19$ years, the total rate of seismic moment release is simply $R^{\max}_{\min} = \frac{1}{\tau}[M_0]^{\max}_{\min}$. For $\beta_1 = 1$, the moment integral diverges as $M_{\max} \to \infty$, which simply means that there is some dimension (if nothing else, the Earth's radius) controlling the maximum size of an earthquake. More realistically, we will use as $M_{\max}$ the moment of the largest deep earthquake ever recorded, 2.6×10^{28} dyn-cm. Similarly, for $\beta_3 = 1$, the moment integral diverges as $M_{\min} \to 0$, which simply expresses that the scaling laws will not be valid below some minimum dimension of the source (if nothing else, the grain size of the material). More realistically, Rundle (1993) has shown that in the case of shallow earthquakes, the existence of a region with inelastic properties (fault gouge) introduces a length scale λ_c in the problem, and results in a Fermi-Dirac frequency-size distribution, which coincides with the Gutenberg-Richter relation only when the characteristic size L of the event is much larger than λ_c. This behavior ensures the convergence of the moment integral. Rundle estimated λ_c to be on the order of a few tens of meters for shallow events, corresponding to a critical moment $M_c = 1.9 \times 10^{18}$ dyn-cm. As detailed below, we will assume that a similar limitation exists for transition zone or deeper earthquakes, even though the nature of the characteristic length λ_c may remain unclear. For practical purposes, we will first compute the seismic moment integral over the interval $\{M_{\text{thresh}}; M_{\max}\}$, and then adjust it to include the contribution of smaller earthquakes obeying the Fermi-Dirac distribution.

We assume that the detection threshold M_{thresh} falls below the critical moment M_2; then, the rate of seismic moment release in the relevant interval is given by:

$$\begin{aligned}
R^{\max}_{\text{thresh}} &= \frac{1}{\tau}\cdot[M_0]^{\max}_{\text{thresh}} = \frac{10^{a_3}}{\tau}\left[\sqrt{\frac{M_1}{M_2}}\left(\ln\frac{M_{\max}}{M_1}+1\right)\right. \\
&\quad \left. + \ln\frac{M_2}{M_{\text{thresh}}} - 1\right] \qquad (4)
\end{aligned}$$

That no earthquake has been located in the deep mantle, above the detection threshold M_{thresh}, simply means that $N(M_{\text{thresh}}) < 1$ or $a_3 < \beta_3 \cdot \log_{10} M_{\text{thresh}}$. In turn this leads to:

$$\begin{aligned}
R^{\max}_{\text{thresh}} &< \frac{M_{\text{thresh}}}{\tau}\left[\sqrt{\frac{M_1}{M_2}}\left(\ln\frac{M_{\max}}{M_1}+1\right)\right. \\
&\quad \left. + \left(\ln\frac{M_2}{M_{\text{thresh}}} - 1\right)\right] \qquad (5)
\end{aligned}$$

Of course, the seismic moment actually released in the deep mantle during the CMT era beyond M_{thresh} is

exactly zero. In this respect, $R^{\max}_{\text{thresh}}$ simply represents the maximum rate of seismic moment release which would be expected to remain undetected during an average 19-yr period, since it would produce less than 1 earthquake in the moment window $\{M_{\text{thresh}}; M_{\max}\}$ during that time.

We have no control over possible values of M_1 and M_2 in (1). These quantities would be related to the size of the seismogenic blobs, and they can only be the subject of speculation. In the following discussions, we will first assign to the lower mantle values adequate for the deepest part of the transition zone ($M_1 = 3 \times 10^{26}$ and $M_2 = 5 \times 10^{24}$ dyn-cm; (Okal and Kirby, 1995)). We will refer to this model as the 'extrapolated estimate', which should provide an order of magnitude of the seismicity expected in the context of a uniformitarian model attempting to maximize the similarity between the two domains under study. On the other hand, we will also study $[M_0]^{\max}_{\text{thresh}}$ as a function of M_1 and M_2, with the simple restrictions $M_2 \geq M_{\text{thresh}}$ and $M_1 \leq M_{\max}$. We will call the bounds on the resulting values of (5) the 'estimated range' of rate of moment release. Figure 3 shows that under these conditions, the extrapolated rate for $R^{\max}_{\text{thresh}}$ is 43 times $\frac{M_{\text{thresh}}}{\tau}$ (or 2.3×10^{24} dyn-cm/yr) with the estimated range varying from 10 to 195 times $\frac{M_{\text{thresh}}}{\tau}$, or from 5.3×10^{23} to 1.0×10^{25} dyn-cm/yr, for the period 1977–1995.

These numbers can be compared to the total rate of seismic moment release during the same time window for earthquakes taking place in the transition zone (400 to 690 km). In that depth range, the total seismic moment release from the CMT catalogue is 4.98×10^{28} dyn-cm, corresponding to a rate of 2.6×10^{27} dyn-cm/yr, 1130 times more than the extrapolated estimate, and 260 to 4900 times the bounds of the estimated range.

Estimating the contributions below M_{thresh}

However, these numbers relate only to that part of the moment released above the detection threshold M_{thresh}. It is possible to extend the comparison by including the contribution of earthquakes at smaller magnitudes. For this purpose, we assume that the events follow a Fermi-Dirac distribution, modified from Rundle's (1993) Equation (26) to reflect the different fractal dimension of the source:

$$N = 10^{(A-1.5m_c)} \cdot \log_{10}\left(1 + 10^{1.5(m_c - m)}\right) \tag{6}$$

which can be rewritten as a function of moment M_0, rather than magnitude, as:

$$N = 10^{(A-3a/2)} M_c^{-1} \log_{10}\left(1 + \frac{M_c}{M_0}\right) \tag{7}$$

where it has been assumed, following Rundle (1993), that the magnitude m is related to seismic moment through:

$$m = \frac{2}{3}\log_{10} M_0 + a \quad (a = -10.73) \tag{8}$$

and the corner moment M_c is obtained by substituting $m = m_c$ in (8). For large moments, this distribution is equivalent to

$$\log_{10} N = z - \log_{10} M_0 \text{ with}$$

$$z = A - \frac{3}{2}a + \log_{10}(\log_{10} e) = A + 15.73. \tag{9}$$

The total seismic moment released between $M_0 = 0$ and $M_0 = M_{\text{thresh}}$ is then

$$[M_0]_0^{\text{thresh}} = \int_{M_0=0}^{M_0=M_{\text{thresh}}} M_0(-dN)$$

$$= 10^z \ln\left(1 + \frac{M_{\text{thresh}}}{M_c}\right). \tag{10}$$

When applying this result to the deep mantle population, we just replace z by a_3 and obtain a contribution

$$[M_0]_0^{\text{thresh}} = 10^{a_3} \ln\left(1 + \frac{M_{\text{thresh}}}{M_c}\right)$$

$$\leq M_{\text{thresh}} \ln\left(1 + \frac{M_{\text{thresh}}}{M_c}\right) \tag{11}$$

so that the total moment release is

$$[M_0]_0^{\max} = \int_{M_0=0}^{M_0=M_{\max}} M_0(-dN) \tag{12}$$

$$\leq M_{\text{thresh}} \left[\sqrt{\frac{M_1}{M_2}}\left(\ln\frac{M_{\max}}{M_1} + 1\right)\right.$$

$$\left. + \left(\ln\frac{M_2}{M_{\text{thresh}}} - 1\right) + \ln\left(1 + \frac{M_{\text{thresh}}}{M_c}\right)\right].$$

When applying (10) to the transition zone population, we note that the populations of deep events are significantly different in the Tonga–Fiji area and in the rest of the world (Giardini, 1984; Frohlich, 1989). Based on the results of Okal and Kirby (1995) for the depth range 500–600 km, adequate constants would be $M_{\text{thresh}} = 10^{24}$ dyn-cm worldwide; $M_1 = 5 \times 10^{26}$ dyn-cm, $M_2 = 6.3 \times 10^{25}$ dyn-cm in Tonga–Fiji; and

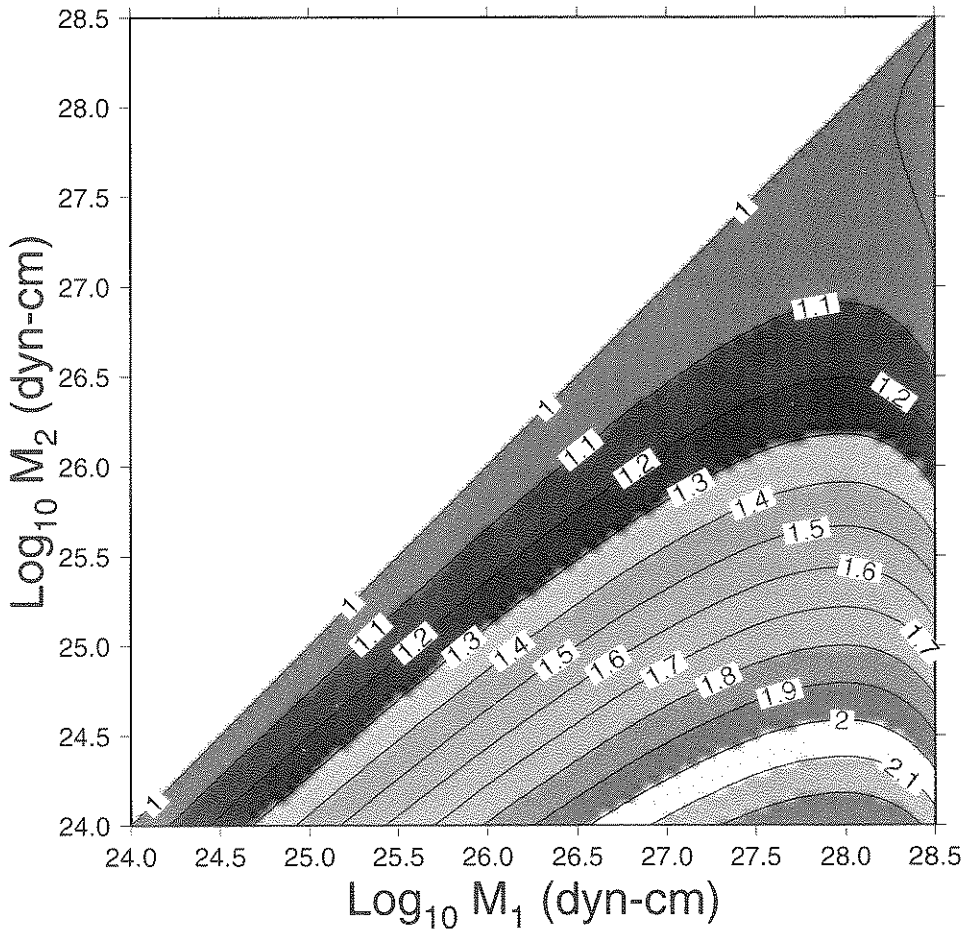

Figure 3. Contoured value of the maximum rate of seismic moment release in the deep mantle, as a function of the corner moments M_1 and M_2 in (1). The function contoured is $\log_{10}\left[\frac{\tau * R_0^{\max}}{M_{\text{thresh}}}\right]$. Thus, for the reference period ($M_{\text{thresh}} = 10^{24}$ dyn-cm; $\tau = 19$ yr), R is found to vary between 5.6×10^{23} and 1.1×10^{25} dyn-cm/yr.

$M_1 = 1.25 \times 10^{26}$ dyn-cm, $M_2 \leq 10^{24}$ dyn-cm outside Fiji (a value much smaller than 10^{24} would probably result in an excessively small width of less than 1 km for the seismogenic zone; thus we will use the upper bound $M_2 = 10^{24}$ dyn-cm outside Fiji). The total CMT moment release beyond M_{thresh} for the transition zone, 4.18×10^{28} dyn-cm outside Fiji and 0.80×10^{28} dyn-cm in Fiji, leads to $z = 26.67$ for Fiji and $z = 26.78$ outside Fiji.

Obviously, it is very difficult, if not impossible, to propose adequate values of M_c, both for the transition zone, and a fortiori, for the deep mantle. We make the simplifying assumption that the critical moments M_c are comparable in the transition zone and the deep mantle. Assuming in turn that the stress drops involved would be of the same order (estimates of stress drops for deep earthquakes vary widely, and obviously we can only speculate as to their possible values in the lower mantle), this amounts to saying that the characteristic lengths λ_c controlling the distribution would be comparable in both regions.

In the case of transition zone earthquakes, it is possible to find a maximum value of M_c based on the observation that the dataset does not exhibit curvature in its frequency-moment relationship for $M_0 \geq M_{\text{thresh}}$. As detailed in Aki (1987) and Rundle (1993), the Fermi-Dirac distribution for shallow earthquakes with $M_c = 1.9 \times 10^{18}$ dyn-cm becomes significantly distinct from its asymptotic Gutenberg-Richter form around $M_0 = 3.9 \times 10^{20}$ dyn-cm, i.e., when the first term neglected in the Taylor expansion of the logarithm in Rundle's (1993) Equation (26) becomes 1% of

the leading term. Since the distribution of transition zone earthquakes does not depart from Gutenberg-Richter behavior for $M_0 \geq 10^{24}$ dyn-cm, we infer $M_c \leq 2 \times 10^{22}$ dyn-cm for that population. On the other hand, a minimum value of M_c remains a matter of speculation. We use here a value of 10^{15} dyn-cm, which is several orders of magnitude below the smallest earthquakes studied at the surface of the Earth. At any rate, an even smaller value of M_c would not significantly change the results which follow.

Using adequate values of the constants z, we have tabulated solutions of (10) as a function of M_c, both for events in the transition zone, and for the possible seismicity of the lower mantle. After adding the contribution beyond M_{thresh}, and in terms of the rate of seismic release $R_0^{\max}$, we find that the extrapolated estimate is increased to between 2.5 and 3.3×10^{24} dyn-cm/yr, while the estimated range would vary between 7×10^{23} and 1.1×10^{25} dyn-cm/yr, depending on the choice of the constants M_c, M_1 and M_2. On the other hand, in the transition zone, the contribution of $M_0 < M_{\text{thresh}}$ would bring the total seismic release rate to anywhere between 2.6 and 3.6×10^{27} dyn-cm/yr, depending on M_c.

Therefore, the maximum seismic moment release rate in the lower mantle (which would still be compatible with fewer than 1 earthquake above M_{thresh} during the reference period), can be expressed as follows, relative to the rate in the transition zone during the same period: extrapolated estimate, about 1000 times less seismic; range of estimates, from 230 to 5100 times less seismic.

Discussion and Conclusion

Since there are no documented earthquakes in the lower mantle, we have had to employ several assumptions to obtain estimates of the maximum rate of seismic moment release, and we need to discuss their robustness in view of the resulting uncertainties.

1. We have assumed in our computations that the threshold moment M_{thresh} fell below the first critical moment M_2 in (1). If on the other hand, the detection threshold takes place in the intermediate regime ($\beta = 1/2$), Equation (5) should be replaced by:

$$R_{\text{thresh}}^{\max} < \frac{M_{\text{thresh}}}{\tau} \left[\sqrt{\frac{M_1}{M_{\text{thresh}}}} \left(1 + \ln \frac{M_{\max}}{M_1} \right) - 1 \right]. \tag{13}$$

In practice, and for all values of M_1 between M_{thresh} and $M_{\max}$, the values of $R_{\text{thresh}}^{\max}$ are changed insignificantly (to between 5.3×10^{23} and 1.0×10^{25} dyn-cm). Finally, should M_{thresh} fall in the high-moment field with $\beta = 1$, i.e., above the larger critical moment M_1, the rate $R_{\text{thresh}}^{\max}$ would be simply expressed by putting $M_1 = M_{\text{thresh}}$ in (10) and $M_1 = M_2 = M_{\text{thresh}}$ in (5).

As for the contribution of the smaller moments below the detection threshold to the maximum moment release rate, we can make the simple argument that inserting a range with $\beta = 1/2$ anywhere below M_{thresh}, while keeping $N(M_{\text{thresh}}) < 1$, would result in a decrease of the number of earthquakes in that range (and consequently of the total seismic moment release), as compared to the case without a $\beta = 1/2$ regime, the latter being covered in the previous analysis, by just putting $M_1 = M_2$ in (12).

Thus, we conclude that the assumption $M_{\text{thresh}} < M_2$ could only have overestimated the seismic release in the lower mantle.

2. Also, in estimating the contribution of very small earthquakes to the total seismic release (10), we have assumed a common value of M_c in the transition zone and in the lower mantle. In principle, the relative rates of seismic release could be affected by a disparity between M_c values in the two regions; however, we found that $R_0^{\max}$ for the lower mantle would be increased at most by a factor of 1.5, *relative* to its counterpart in the transition zone, in the case of two independent values of M_c varying freely in the interval chosen above (10^{15} to 2×10^{22} dyn-cm).

3. A final question to be addressed is that of the influence of having used a rather short reference time window – the 19 years from 1977 to 1995, which is presently the only period during which a homogeneous catalog is available. From the catalog of Huang et al. (1997), covering the 'WWSSN era' (1962–1976), it is suggested that the average rate of deep seismic moment release was indeed comparable during those years, with a total release of 4.2×10^{28} dyn-cm, this figure being complete down to 2×10^{25} dyn-cm, rather than 10^{24} for the CMT era. Note however, that this similarity is nearly exclusively the result of two gigantic earthquakes: the Colombian event during the WWSSN years and the Bolivian one during the CMT era.

Since world-wide detection capabilities have not changed significantly between 1964 (when the WWSSN was completed) and 1977, it is probably safe to interpret the observed aseismicity of the lower man-

tle during 1964–1995 as indicating that no earthquake with $M_0 \geq 10^{24}$ dyn-cm took place during that period. The maximum rates $R_{\text{thresh}}^{\text{max}}$ (5), and consequently the estimates for R_0^{max}, can thus be adjusted by a factor 19/32, the extrapolated estimate falling to between 1.5 and 2.0×10^{24} dyn-cm/yr, while the range of estimates would be 4.2×10^{23} to 6.5×10^{24} dyn-cm/yr. It is not possible to extend this analysis further back in time, since detection capabilities changed drastically in the early 1960s.

By comparing with the long-term rate of activity in the transition zone, we conclude that the lower mantle is at least 400 to 8000 times (with an extrapolated estimate of at least 1700 times) less seismic than the transition zone.

These numbers can then be compared to the variation in seismic activity with depth above 690 km. Figure 4 compares schematically the values of total seismic moment release during the CMT era for three depth bins: the uppermost 70 km corresponding roughly to 'shallow' earthquakes, the upper mantle from 70 to 400 km, the transition zone between 400 and 690 km. Once again, these estimates are based on the CMT dataset, which suffers from its short time span. However, it clearly underestimates both shallow and deep events (the largest CMT solution to date, the 1977 Indonesian earthquake, is about 100 times smaller than the biggest event ever detected – the 1960 Chilean earthquake). In round numbers, the upper mantle is found to be about 7 times less seismic than the band of shallow earthquakes; seismicity in the transition zone drops by another factor of 3. However, the transition to the lower mantle is clearly different, since it involves at least 3 orders of magnitude less seismic activity.

Thus, any lower mantle seismic release must be limited to very low levels, even when detection limits are factored in. At least some subducting slabs appear to penetrate into the lower mantle, and, while a subset of proposed failure mechanisms cannot operate in the $pv + mw$ field, we know of no reason why all potential mechanisms for seismic stress release suddenly should cease to operate below 690 km depth. We suggest, therefore, that an absence of significant accumulated strain energy below this depth is responsible for the observed low seismic potential of the lower mantle. Both the absence of major phase transitions, with attendant buoyancy anomalies for generating deviatoric stresses, at greater depths and the inability of a fine-grained, weak, superplastic $pv + mw$ zone to accumulate significant strain energy at greater depths are consistent with this interpretation.

Appendix

We present here individual discussions of the relocation of all events given a NEIC location deeper than 690 km, and posterior to Stark and Frohlich's (1985) study, and of those historical events whose depths Rees and Okal (1987) were unable to constrain.

Post-1980 events: $h_{\text{NEIC}} > 690$ *km*

• *12 April 1984; Original location:* 24.124° *S;* 179.004° *E; 694 km;* $m_b = 4.6$

The NEIC location results in an unacceptable residual at Nadi (–16.6 s). The dataset of 10 P times converges on 23.95° S, 179.49° E, at a depth of 561 km, with no residuals exceeding 1.7 s. This solution is equivalent to the ISC's.

• *10 January 1985; Original location:* 18.039° *S;* 178.501° *W; 701 km*

The NEIC location is incompatible with the arrival times at the stations in Fiji and results in a standard deviation of 3.49 s. The dataset of 23 arrival times converges on 18.10° S, 178.13° W at 646 km (σ = 0.92 s), in excellent agreement with the ISC location.

• *22 October 1985, 19:14 GMT; Original location:* 20.158° *S;* 179.163° *W; 700 km;* $m_b = 5.5$

The ISC location is given a depth of 695 ± 13 km. The Harvard CMT solution is at 684 km. The dataset of 32 arrival times converges on 685 km, but the depth resolution is weak. A Monte Carlo test injecting noise with σ_G of just 1 s scatters the hypocentral depths from 664 to 700 km. The combination of our relocation, the ISC solution and the CMT depth suggest that this event is probably at the very bottom of the subduction zone 685 km ± 10 km). There is no reason to favor a deeper source, such as the NEIC depth.

• *22 October 1985, 19:29 GMT. Original location:* 20.123° *S;* 179.309° *W; 707 km*

This aftershock of the previous event is also given at 707 km by the ISC. The dataset of 17 arrival times converges on 710 km (σ = 0.47 s), but there is little depth resolution with Monte Carlo relocations (σ_G = 1 s) ranging in depth from 686 to 733 km. We prefer hold-

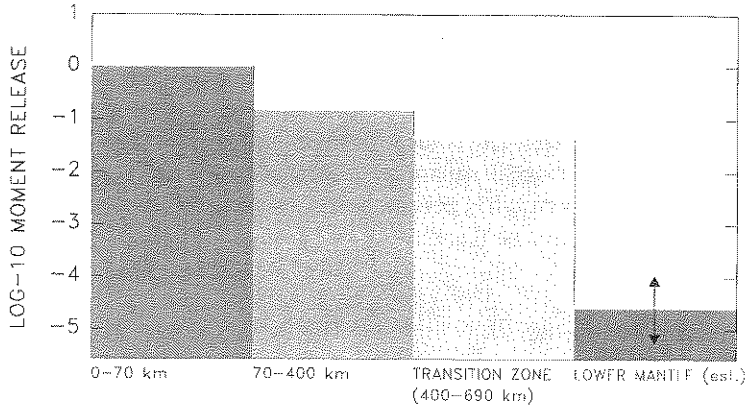

Figure 4. Comparison of the rates of seismic moment release for various depth ranges. The first three bars at the left were derived from the Harvard CMT file (1977–1995); the fourth one illustrates the maximum possible level of activity of the lower mantle, as derived in our study, and relative to the activity in the transition zone. The bar is drawn at the extrapolated estimate (1700 times less seismic than the lower mantle), and the arrows show the range of estimates (400 to 8000 times less seismic). Absolute vertical scale arbitrary.

ing the depth at 690 km, which results in a perfectly acceptable solution ($\sigma = 0.76$ s).

• *09 May 1989; Original location:* 17.694° *S;* 179.091° *W; 692 km*

This event, labeled 'poor solution' by the NEIC, is given at 693 km by the ISC but with very poor depth resolution (±43 km). Our solution converges on 685 km, the standard deviation being only 0.01 s smaller than at 693 km, and the hypocenters from the Monte Carlo runs ($\sigma_G = 1$ s) are scattered from 631 to 735 km. There is no reason to believe that the earthquake is anomalously deep.

• *08 November 1989; Original location:* 19.695° *S;* 178.749° *W; 707 km*

This small event is listed at 710 ± 19 km by the ISC. Our relocation converges on 709 km ($\sigma = 0.27$ s), but a solution at a constrained depth of 690 km is also excellent ($\sigma = 0.65$ s). The Monte Carlo runs ($\sigma_G = 1$ s) yield depths ranging from 678 to 733 km.

• *19 May 1992; Original location:* 21.974° *S;* 178.558° *W; 696 km*

This event is located by the ISC at a much shallower location (282 km), with a precision (±17 km) which clearly indicates that the PDE estimate was erroneous. This intermediate depth is also confirmed (280 km) by our relocation.

• *29 December 1992; Original location:* 20.33° *S;* 178.95° *W; 695 km*

This relatively small event ($m_b = 4.4$) is listed at 665 ± 49 km by the ISC. Our relocation converges on a similar value of 664 km when station MBL is eliminated (its residual with respect to the final location is –17.6 s). However, depth resolution is poor, as indicated both by the ISC error bar and by the range of Monte Carlo hypocenters (620 to 729 km).

Historical events; $h_{NEIC} \geq 670$ km

• *25 August 1933; Original location:* 6° *S;* 121° *E; 720 km; M = 6.5 (G–R)*

Note that the ISS lists this event as shallow. We were unable to find any readable records of this earthquake, which took place 90 mn after a much stronger event in Sichuan ($M_{PAS} = 7.4$). The times at the closest station, Amboina, are generally incompatible with the remainder of the data, but increasing them by one minute leads to a satisfactory solution at 6.1° S; 120.8° E, $h = 607$ km with $\sigma = 2.56$ s on 9 stations. However, the dataset has no depth resolution, with Monte Carlo hypocenters ($\sigma_G = 4$ s) ranging from 160 to 751 km depth. The earthquake is probably deep, but there is no reason to give it an anomalously deep focus.

• *20 December 1939; Original location* 7° *S;* 120° *E; 700 km;* $M = 6$

Based on BCIS and ISS times, we propose to relocate this event at 6.95° S; 121.10° E; 623 km. The solution uses 11 stations and achieves a root-mean square residual $\sigma = 1.95$ s. The solution, however, has poor depth control, but there is no reason to assume that the earthquake is anomalously deep.

• *13 November 1954; Original location* 30° *N;* 131.8° *E; 800 km*

BCIS data ($h = 80$ km) confirm that the NEIC listing is the result of a typographic error. We relocate the event at 62 km depth.

• *18 November 1954; Original location* 42.25° *N;* 141.6° *E; 800 km*

BCIS data ($h = 80$ km) confirm that the NEIC listing is the result of a typographic error. We relocate the event at 89 km depth.

• *21 January 1956; Original location:* 1.5° *S;* 129.5° *E; 700 km*

The NEIC location is intriguing since only shallow seismicity is documented in that part of the Ceram Sea. We suggest that the P time at Brisbane is one minute fast, while the S time at Matsushiro is one minute slow. On this basis, we relocate the event further South, in the eastern arc of the Banda Sea, at {5.49° S; 130.08° E; $h = 186$ km}, with $\sigma = 0.75$ s on 7 stations.

• *12 March 1957; Original location:* 21.5° *S;* 179° *W; 700 km*

A solution based on 19 P and S times from the BCIS converges on 21.11° S, 178.80° W at 681 km, with $\sigma = 2.67$ s. The dataset does not warrant locating this earthquake any deeper, even though the Monte Carlo hypocenters ($\sigma_G = 2$ s) do extend to 706 km,

• *10 October 1957; Original location:* 22° *S;* 178.5° *W; 700 km*

While the dataset of 15 P times converges on a solution at 712 km ($\sigma = 1.23$ s), there is little depth resolution, and the solution does not deteriorate significantly if the depth is constrained at 690 km ($\sigma = 1.45$ *s*). Inclusion of 3 regional S times moves the unconstrained solution to 708 km ($\sigma = 2.43$ s), but a depth of 690 km is practically as good ($\sigma = 2.57$ s). This depth is also in excellent agreement with reported $pPKP$ and PKP times at Helwan. The hypocentral depths of Monte Carlo runs ($\sigma_G = 2$ s) range from 680 to 744 km.

• *14 July 1959; 18:20 GMT; Original location* 21° *S;* 179° *W; 700 km (BCIS)*

This event is an aftershock of a larger earthquake which occurred 6 mn earlier. The main shock is listed at 620 km on the NEIC tape (they use a location by Sykes) and 700 km by the BCIS. We relocated it at 627 km. Only 6 times are listed by the BCIS for the aftershock, one of them (Adelaide) incompatible with the rest. This dataset cannot resolve depth (with Monte Carlo depths ranging from 595 to 752 km; $\sigma_G = 1.5$ s), but a solution constrained at 627 km is perfectly acceptable ($\sigma = 0.53$ s).

• *07 April 1960; Original location* 21.37° *S;* 179.29° *W; 670 km (NEIC)*

This event is given an approximate depth of 600 km by the BCIS. We relocate it at 585 km based on 9 stations listed in the BCIS. The Monte Carlo depths ($\sigma_G = 1.5$ s) range from 502 to 642 km and would exclude the deepest part of the WBZ.

• *11 November 1960; Original location* 19.84° *S;* 179.05° *W; 670 km (NEIC)*

The BCIS lists this event simply as having 'discordant data'. We suggest that Canberra and Charter Towers were running 1 minute fast, and that the reading at Broken Hill is unrelated to this event; this adjustment yields an excellent solution ($\sigma = 0.72$ s on 12 stations) at 666 km depth, fundamentally undistinguishable from the NEIC hypocenter. Monte Carlo depths range from 626 to 704 km ($\sigma_G = 1.5$ s).

Acknowledgements

We thank Steve Kirby for discussions and Bob Engdahl for access to his relocation catalogue in advance of publication. The paper benefited from careful reviews by Cliff Frohlich and Steve Kirby. This research was supported by the National Science Foundation under Grant EAR-93-16396.

References

Adams, 1963. Source characteristics of some deep New Zealand earthquakes, *N.Z. J. Geol. Geophys.* **6**, 209–220.

Adams, R. D., and Ferris, B. G., 1976. A further earthquake at exceptional depth beneath New Zealand, *N.Z. J. Geol. Geophys.* **19**, 269–273.

Aki, K., 1987. Magnitude-frequency relation for small earthquake: a clue to the origin of f_{max} of large earthquakes, *J. Geophys. Res.* **92**, 1349–1355.

Bevis, M., Taylor, F. W., Schutz, B. E., Recy, J., Isacks, B. L., Helu, S., Singh, R., Kendrick, E., Stowell, J., Taylor, B. and Calmant, S., 1995. Geodetic observations of very rapid convergence and back-arc extension at the Tonga arc, *Nature* **374**, 249–251.

Bina, C. R., 1996. Phase transition buoyancy contributions to stresses in subducting lithosphere, *Geophys. Res. Lett.* **23**, 3563–3566.

Bina, C. R., 1997. Patterns of deep seismicity reflect buoyancy stresses due to phase transitions, *Geophys. Res. Lett.* **24**, 3301–3304.

Bina, C. R. and Helffrich, G., 1994. Phase transition Clapeyron slopes and transition zone seismic discontinuity topography, *J. Geophys. Res.* **99**, 15,853–15,860.

Chase, C. G., 1971. Tectonic history of the Fiji Plateau, *Geol. Soc. Amer. Bull.* **82**, 3087–3110.

Chung, W.-Y., and Kanamori, H., 1976. Source process and tectonic implications of the Spanish deep earthquake of March 29, 1954, *Phys. Earth Planet. Inter.* **13**, 85–96.

Dziewonski, A. M., Friedman, A., Giardini, D. and Woodhouse, J. H., 1983. Global seismicity of 1982: Centroid moment tensor solutions for 308 earthquakes, *Phys. Earth Planet. Inter.* **33**, 76–90.

Engdahl, E. R., van der Hilst, R. D. and Buland, R. P., 1997. Global teleseismic earthquake relocation with improved travel times and procedures for depth determination, *Bull. Seismol. Soc. Amer.*, in press.

Engebretson, D., and Kirby, S., 1992. Deep Nazca slab seismicity: why is it so anomalous?, *Eos, Trans. Amer. Geophys. Un.* **73**, (43), 379 (abstract).

Engebretson, D. C., Mammerickx, J. and Raymond, C. J., 1991. Tonga lineations: the Phoenix Plate has arisen?, *Eos, Trans. Amer. Geophys. Un.* **72**, (44), 444 (abstract).

Frohlich, C., 1989. The nature of deep-focus earthquakes, *Ann. Rev. Earth Planet. Sci.* **17**, 227–254.

Giardini, D., 1984. Systematic analysis of deep seismicity: 200 centroid-moment tensor solutions for earthquakes between 1977 and 1980, *Geophys. J. Roy. Astr. Soc.* **77**, 883–914.

Hamburger, M. W., and Isacks, B. L., 1987. Deep earthquakes in Southwest Pacific: A tectonic interpretation, *J. Geophys. Res.* **92**, 13841–13854.

Huang, W.-C., 1996. Centroid-moment tensor inversions of analog seismograms from deep earthquakes (1907–1976), Ph.D. dissertation, Northwestern University, 193 pp.

Huang, W.-C., Ekström, G., Okal, E. A. and Salganik, M. P., 1994. Application of the CMT algorithm to analog recordings of deep earthquakes, *Phys. Earth Planet. Inter.* **83**, 283–297.

Huang, W.-C., Okal, E. A., Ekström, G. and Salganik, M. P., 1997. Centroid-Moment-Tensor solutions for deep earthquakes predating the digital era: The WWSSN dataset (1962–1976), *Phys. Earth Planet. Inter.* **99**, 121–129.

Ito, E. and Sato, H., 1991. Aseismicity in the lower mantle by superplasticity of the descending slab, *Nature* **351**, 140–141.

Ito, E. and Sato, H., 1992. Effect of phase transformations on the dynamics of the descending slab, in Syono, Y. and Manghnani, M. H. (eds), *High-Pressure Research: Application to Earth and Planetary Sciences, Amer. Geophys. Un.*, Washington, D.C., pp. 257–262.

Jeffreys, H. and Bullen, K. E., 1940. Seismological tables, Brit. Assoc. Adv. Sci., London, 43 pp.

Karato, S., 1997. Phase transformations and rheological properties of mantle minerals, in Earth's Deep Interior: The Doornbos Memorial Volume, ed. D. J. Crossley, Gordon and Breach, Amsterdam, pp. 223–272.

Karato, S., 1998. Seismic anisotropy in the deep mantle, boundary layers and the geometry of mantle convection, *Pure Appl. Geophys.*, in press.

Kennett, B. L. N., Engdahl, E. R. and Buland, R., 1995. Constraints on seismic velocities in the Earth from travel times, *Geophys. J. Intl.* **122**, 108.

King, S. D., 1995. Models of mantle viscosity, in Ahrens, T. J. (ed.), *Mineral Physics & Crystallography, AGU Ref. Shelf 2, Amer. Geophys. Un.*, Washington, D.C., pp. 227–236.

Kirby, S. H. and Okal, E. A., 1996. Geodynamic Implications of Deep Earthquakes in Slabs Stagnated in the Transition Zone: Deep Seismicity Beneath the Fiji Basin, SW Pacific, *Eos, Trans. Amer. Geophys. Un.* **77**, (46), F498 (abstract).

Kirby, S. H., Durham, W. B. and Stern, L. A., 1991. Mantle phase changes and deep-earthquake faulting in subducting lithosphere, *Science* **252**, 216–225.

Kirby, S. H., Stein, S., Okal, E. A. and Rubie, D., 1996. Deep earthquakes and metastable mantle phase transformations in subducting oceanic lithosphere, *Rev. Geophys. Space Phys.* **34**, 261–306.

Kostoglodov, V. V., 1989. Maximal'naya glubina zemletryasenii i fazovye prevrashcheniya v litosfere, pograzhayushchejsya v mantiyu, in Magnitskii, V. A., *Fizika i vnutrennee stroienie zemli*, Nauka, Moskva, pp. 52–57 (in Russian).

Lundgren, P. and Giardini, D., 1992. Seismicity, shear failure and modes of deformation in deep subduction zones, *Phys. Earth Planet. Inter.* **74**, 63–74.

Marton, F. C., Bina, C. R., Stein, S. and Rubie, D. C., 1997. Are all Φs created equal?, *Eos, Trans. Amer. Geophys. Un.* **78**, (48), F662. (abstract).

Myers, S. C., Wallace, T. C., Beck, S. L., Silver, P. G., Zandt, G., Van Decar, J. and Minaya, E., 1995. Implications of spatial and temporal development of the aftershock sequence of the $M_w = 8.3$ June 9, 1994 deep Bolivian earthquake, *Geophys. Res. Lett.* **22**, 2269–2272.

Navrotsky, A., 1980. Lower mantle phase transitions may generally have negative pressure-temperature slopes, *Geophys. Res. Lett.* **7**, 709–711.

Okal, E. A., 1992. A student's guide to long-period body-wave amplitudes, *Seismol. Res. Lett.* **63**, 169–180.

Okal, E. A., 1993. m_b: A theoretical attempt at modeling the depth-distance correction, *Eos, Trans. Amer. Geophys. Un.* **74**, (16), 204 (abstract).

Okal, E. A. and Bina, C. R., 1994. The deep earthquakes of 1921–1922 in Northern Peru, *Phys. Earth Planet. Inter.* **87**, 33–54.

Okal, E. A. and Kirby, S. H., 1995. Frequency-moment distribution of deep earthquakes: Implications for the seismogenic zone at the bottom of slabs, *Phys. Earth Planet. Inter.* **92**, 169–187.

Parsons, B. and Sclater, J. G., 1977. An Analysis of the variation of ocean floor bathymetry and heat flow with age, *J. Geophys. Res.* **82**, 803–827.

Rees, B. A. and Okal, E. A., 1987. The depth of the deepest historical earthquakes, *Pure Appl. Geophys.* **125**, 699–715.

Rundle, J. B., Magnitude-frequency relations for earthquakes using a statistical mechanical approach, *J. Geophys. Res.* **98**, 21943–21949.

Russakoff, D., Ekström and Tromp, J., 1997. A new analysis of the great 1970 Colombia earthquake and its isotropic component, *J. Geophys. Res.* **102**, 20423–20434.

Schubert, G., Yuen, D. A. and Turcotte, D. L., 1975. Role of Phase Transitions in a Dynamic Mantle, *Geophys. J. R. Astr. Soc.* **42**, 705–735.

Stark, P. B. and Frohlich, C. H., 1985. The depths of the deepest deep earthquakes, *J. Geophys. Res.* **90**, 1859–1869.

Stein, C. A. and Stein, S., 1992. A model for the global variation in oceanic depth and heat flow with lithospheric age, *Nature* **359**, 123–129.

Van der Hilst, R. D., 1995. Complex morphology of subducted lithosphere in the mantle beneath the Tonga trench, *Nature* **374**, 154–157.

Van der Hilst, R. D. and Engdahl, E. R., 1992. Step-wise relocation of ISC earthquake hypocenters for linearized tomographic imaging of slab structure, *Phys. Earth Planet. Inter.* **75**, 39–53.

Van der Hilst, R. D., Engdahl, E. R., Spakman, W. and Nolet, G., 1991. Tomographic imaging of subducted lithosphere below Northwest Pacific island arcs, *Nature* **353**, 37–43.

Van der Hilst, R. D., Widiyantoro, S. and Engdahl, E. R., 1997. Evidence for deep mantle circulation from mantle tomography, Nature, in press.

Weidner, D. J., 1997. Rheological properties of mantle minerals: Implications for deep focus earthquakes, *Eos, Trans. Amer. Geophys. Un.* **78**, (17), S215 (abstract).

Wysession, M. E., Okal, E. A. and Miller, K. L., 1991. Intraplate seismicity of the Pacific Basin, 1913–1988, *Pure Appl. Geophys.* **135**, 261–359.